Chapter 2
Supercritical Water Process

Abstract Hydrothermal synthesis of particles is usually carried out at subcritical conditions in batch reactors. In supercritical region, reaction rate increases dramatically due to low dielectric constant (ε) of SCW. Therefore, fine particles (e.g., metal oxides) are rapidly synthesized (e.g., 0.4 s∼2 min) in a continuous SCW process. In the oxide synthesis, an ionic metal salt is first hydrolyzed to metal hydroxide, which is then dehydrated to form metal oxide crystals by precipitating from SCW solution. Here, three types of reactors (batch, flow and diamond anvil cell) are introduced in details for the study of SCW synthesis of particles. In general, batch reactors are used for long time process, and flow reactors for short time synthesis. Diamond anvil cell is used for in-situ visual and spectroscopic study of particle formation. Continuous flow reactors allow a better control of experimental conditions (e.g., temperature, pressure, time, concentration, pH and heating rate) that lead to formation of smaller particles with uniform size.

2.1 Introduction

Conventional methods prepared for oxide particles are high temperature solid-state reaction (SSR) [1, 2], high-energy ball milling [3] sol-gel [1, 4, 5], microemulsion methods [6, 7], oxidation techniques [8] and co-precipitation with ageing of solutions [9, 10]. However, many of these processes are energy- and time-consuming (high temperature, multi-step syntheses or ageing) and environmentally unfriendly [11]. Hydrothermal (sub- or super-critical water) synthesis is another method to produce fine particles. This process has been carried out since the end of the nineteenth century, mainly in the production of synthetic minerals to imitate natural geothermal processes [12, 13]. Since then many highly crystalline metal oxides have been produced [11]. However, most of the syntheses were undergone long-time reaction in batch reactors in SubCW conditions [14, 15]. Continuous SCW synthesis is a relative novel technique to produce fine particles. Arai and Adschiri (1992, Tohoku University, Japan) pioneered the rapid one-step synthesis of metal oxide nano-crystals in SCW in continuous flow reactors [16, 17].

Z. Fang, *Rapid Production of Micro- and Nano-particles Using Supercritical Water*, Engineering Materials 30, DOI 10.1007/978-3-642-12987-2_2,

In the process of hydrothermal synthesis, low-cost precursors (e.g., nitrate or acetate salts, hydroxides) are first dissolved in water. The salt solution is introduced into a reactor operated at sub- or super-critical conditions. This method has a potential to adjust the direction of crystal growth, morphology, particle size and size distribution, because of the controllability of thermodynamics and transport properties by pressure and temperature. The synthesis reactions taking place in the reactor are considered to be as follows [17, 18]:

$$MeL_x + x\ H_2O \rightarrow Me(OH)_x + x\ HL \tag{2.1}$$

$$Me(OH)_x \rightarrow MeO_{x/2} \downarrow + x/2\ H_2O \tag{2.2}$$

$$MeO_{x/2} + x/2\ H_2 \rightarrow Me + x/2\ H_2O \tag{2.3}$$

where $L = NO_3^-$, CH_3COO^- or other anions; Me = metal.

In Eq. (2.1), metal salt is first hydrolyzed to metal hydroxide, which is then dehydrated, according to Eq. (2.2), forms metal oxide crystals with micro- or nano-size by precipitating from the solution. Metal particles can be produced by hydrogen reduction of the metal oxide particles (Eq. 2.3) [18]. In an isobar (Fig. 1.9), K_w or $[OH^-]$ concentration increases significantly upon reaching supercritical region. Therefore, SCW promotes hydrolysis reaction (Eq. 2.1) and enhances production of oxide particle. These reactions (Eqs. 2.1, 2.2, and 2.3) also explain how to remove water-soluble heavy metal cations and recover metal oxides using hydrothermal SCW techniques [19, 20].

In our previous work [20], water-soluble heavy metal cations (100% Pb, 97.6% Cd, and 87.3% Cr) were converted to water-insoluble particles during SCW oxidation (SCWO) of organic wastes. In addition to the formation of metal oxides (Eqs. 2.1, 2.2, and 2.2), it was found that CO_2 and acetate from SCWO of organics could help to remove heavy metal cations via formation of water insoluble carbonate salts (Eq. 2.4). X-ray diffraction (XRD) spectra indicated the presence of $PbCrO_4$ and $Al_2Si_2O_5(OH)_4$ crystals in the ash (Fig. 2.1).

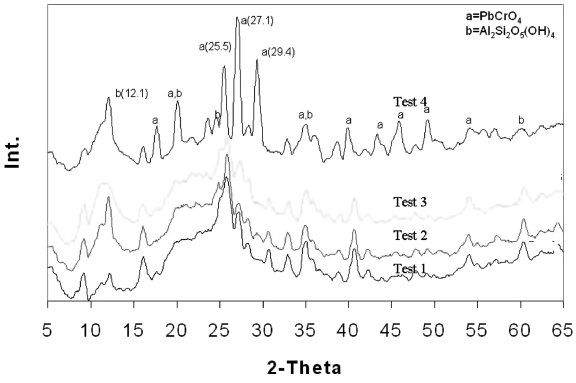

Fig. 2.1 XRD spectra of ashes from SCWO of organic wastes with heavy metal cations (tests 1–4 at different temperatures & excessive O_2). Reprinted with permission from [20]. Copyright © 2000, American Chemical Society

Super-probe electron probe micro-analyzer (EPMA) results showed the ash contained very fine and highly concentrated Pb (4.4–75.3%), and a close connection between Pb and Cr but no relation between Pb and Cd in the ash (Fig. 2.2). In most of the locations where Pb was present, Cr was also seen, but no Cd was detected (Fig. 2.2a, b, points A–E, and Fig. 2.2d, e, point A). The main solid fine particles were CdO, $CdCO_3$, CrO_2, $HCrO_2$, $PbCrO_4$, $PbCO_3$ and PbO_x. In SCWO of organics, more reactions are likely to follow:

$$MeO_{x/2} + CO_2 \rightarrow Me(CO_3)_y \downarrow \tag{2.4}$$

$$CrO_2 + O_2 \rightarrow CrO_4^{2-} \tag{2.5}$$

$$Pb^{2+} + CrO_4^{2-} \rightarrow PbCrO_4 \downarrow \tag{2.6}$$

Hydrothermal synthesis of fine crystal particles in SCW is a rapid process. Adschiri et al. [21] explained the higher synthesis reaction rate in SCW due to its low dielectric constant (ε) as compared with the rate in SubCW, according to the theory of Born:

$$\ln k = \ln k_0 - (\omega/R)(1/\varepsilon - 1/\varepsilon_0)/T \tag{2.7}$$

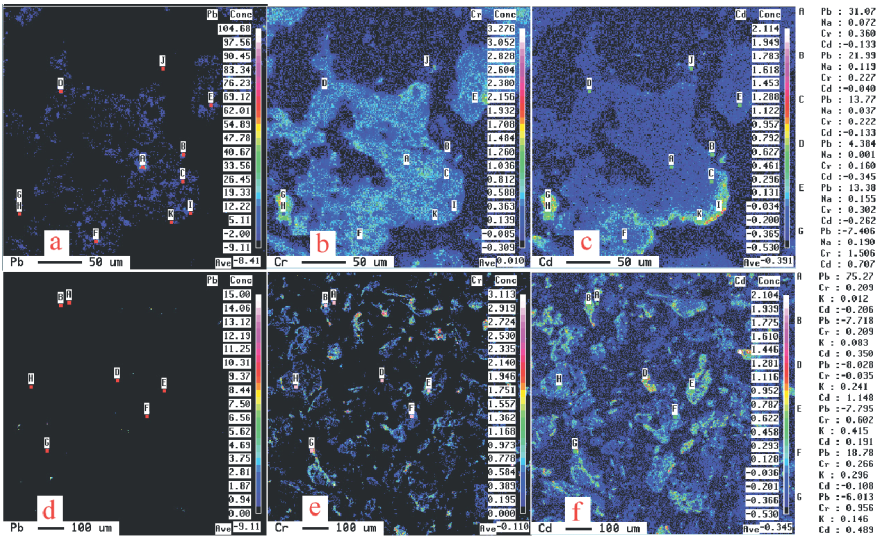

Fig. 2.2 EPMA images of analytical results for the selected ash: (i) a small particle (50 μm): **a** (Pb), **b** (Cr), **c** (Cd); (ii) a large mapping area (100 μm): **d** (Pb), **e** (Cr), **f** (Cd). Reprinted with permission from [20]. Copyright © 2000, American Chemical Society

where ω – constant determined by a reaction system (> 0); ε – dielectric constant; k – reaction rate constant; k_0 – reaction rate at constant dielectric constant ε_0 and T_0.

As temperature increases to SCW region from an initial temperature T_0, ε drops significantly (Fig. 1.8), thus $(1/\varepsilon - 1/\varepsilon_0)$ increases sharply (Fig. 2.3). So, ln k vs. 1/T [slope: $(\omega/R) \bullet (1/\varepsilon - 1/\varepsilon_0)$] rises greatly according to Eq. 2.7. Experiments were carried out to verify the Eq. 2.7 at different reaction time (τ) and temperature for the aqueous solution of $Al(NO_3)_3$ (0.01 mol/L) system at 30 MPa in a flow reactor [21]. The $[Al^{3+}]$ conversion rate, X was calculated by measuring its concentration changes in the effluent. The rate constant (k) was obtained in Fig. 2.4 from the slope of $-\ln(1 - X)$ vs. τ. Therefore, Arrhenius first order plot of ln k with 1/T was given as showed in Fig. 2.5.

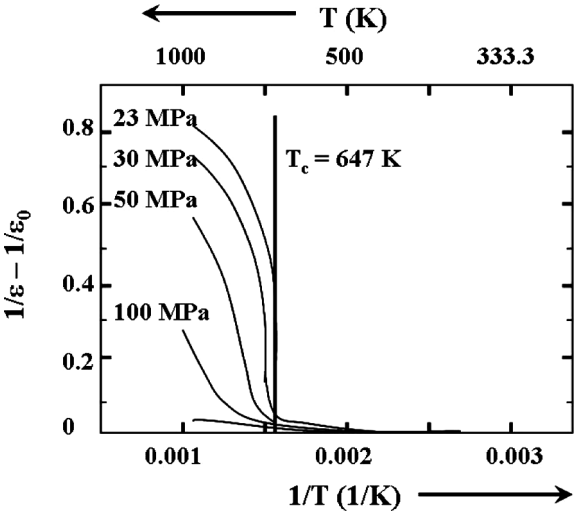

Fig. 2.3 $(1/\varepsilon - 1/\varepsilon_0)$ plotted against 1/T. Reprinted with permission from [21]. Copyright © 2000, American Chemical Society

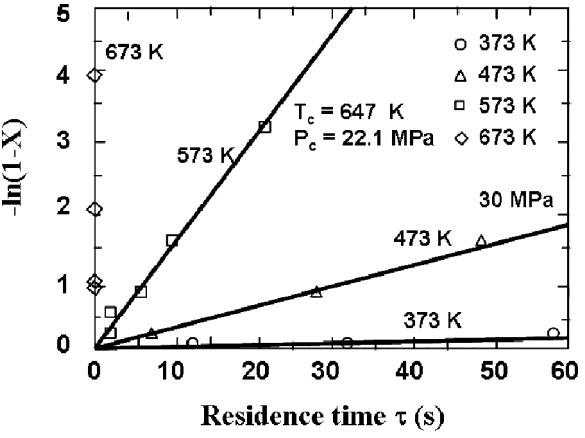

Fig. 2.4 $-\ln(1-X)$ vs. time curves at 30 MPa for $Al(NO_3)_3$ (0.01 mol/L). Reprinted with permission from [21]. Copyright © 2000, American Chemical Society

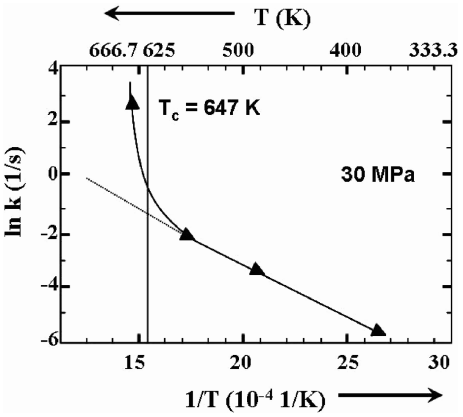

Fig. 2.5 Arrhenius plot of the apparent first-order rate constant at 30 MPa for $Al(NO_3)_3$. Reprinted with permission from [21]. Copyright © 2000, American Chemical Society

In the range of subcritical temperature, the rate constant fell on a straight line, but increased significantly above the critical temperature. This enhancement in rate in the critical region confirms the result predicted by Eq. (2.7). Synthesis of oxide fine particles in SCW is a rapid process (typically from 0.4 s to 2 min) in a continuous flow reactor.

It is important to have appropriate reactors to do experiments. Three types of reactors, batch, flow and diamond anvil cell (DAC) are introduced next for different applications and purposes in fine particle production.

2.2 Batch Reactor

Batch and flow reactors are widely used for the hydrothermal processes. The batch reactor could be an autoclave heated by an electric heater (Fig. 2.6; FCFD05-30, Yantai Jianbang chemical mechanical Co., Ltd. Shandong, China) or a tubular reactor heated by a salt bath (or fluidized sand bed) (Fig. 2.7). Owing to slow heating rates in autoclaves (e.g., 0.18 K/s; 30 min heated to 623 K from room temperature), smaller tubular reactors with higher heating rates heated by a fluidized sand bath (e.g., 5.4 K/s; 2 min heated to 673 K from room temperature) are widely used in SCW reactions (Fig. 2.7). The 316 stainless-steel (SS) or inconel tubular batch reactor (6 mL; length of 105 mm, OD of 12.7 μm, ID of 8.5 μm) is widely used to investigate hydrothermal reactions. The reactor is connected to a transducer (Dynisco E242) for on-line pressure and temperature (J-type thermocouple) measurements, as well as to a data acquisition system (Strawberry tree, DS-12-8-TC). Both the transducer and the reactor can be used up to 35 MPa at 811 K.

Solid or liquid samples and water are loaded into the reactor. After being sealed and connected to the data acquisition system, the reactor is submerged in a fluidized sand bath (Omega FSB-3), where temperature can be controlled up to 873 K within 1 K. The uniformity of the sand temperature is within 0.5 K. The sample is heated at a rate of 3.5 K/s up to 873 K. Figure 2.8 gives an example of temperature

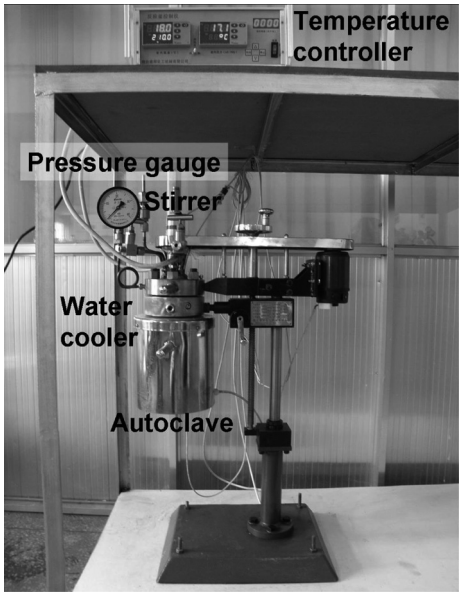

Fig. 2.6 Photograph of a commercial autoclave set-up in our Lab

and pressure profiles measured at different fluidized bed temperature (FBT) with or without loading H_2O_2 (49 wt%, 1 mL). H_2O_2 will decompose to H_2O and O_2 (mainly at low temperature of 426 K) [22]. Usually pressure can also be calculated by an equation of state of water (EOSW) [23] by knowing temperature measured and water density (ρ = water mass/reactor volume; kg/m^3).

After reactions, the reactor is quenched in cold water. The reactor is then connected to a 500-mL syringe for the collection and volume measurements of the gas phase generated during reactions. The gas is analyzed by Gas Chromatograph-Thermal Conductivity Detector (GC-TCD). The reaction mixture is separated into three phases: (1) aqueous phase (10 mL), which is obtained by washing products with water *via* 25-nm pore size membrane filter; (2) acetone or benzene phase (10 mL), which is obtained by washing the remainder with acetone or benzene; and (3) fine particles, collected on the filter paper (or separated by using a super-speed centrifuge) and dried at 373 K for 24 h. The aqueous phase is analyzed for anion and metal ion concentrations using Ion Chromatograph (IC) and Inductively Coupled Plasma spectrometry (ICP), respectively, in order to estimate the conversion rate for the fine particles synthesized. The acetone or benzene phase is analyzed by High-Pressure Liquid Chromatography (HPLC) and GC-Mass Spectrometry (GC-MS). Fine particles are analyzed their elemental distribution by an EPMA and Energy Dispersive X-Ray spectrometry (EDX), their structure is analyzed by XRD. The particles are also characterized by Dynamic Light Scattering (DLS), Mössbauer Spectroscopy, Fourier Transform Infrared (FTIR)/Raman Microscopy, Transmission Electron Microscope (TEM), Scanning Electron Microscopy (SEM), Micromeritics Surface Area and Pore Size Analyzer, Differential Scanning Calorimeter (DSC) and Thermogravimetric Analysis (TGA).

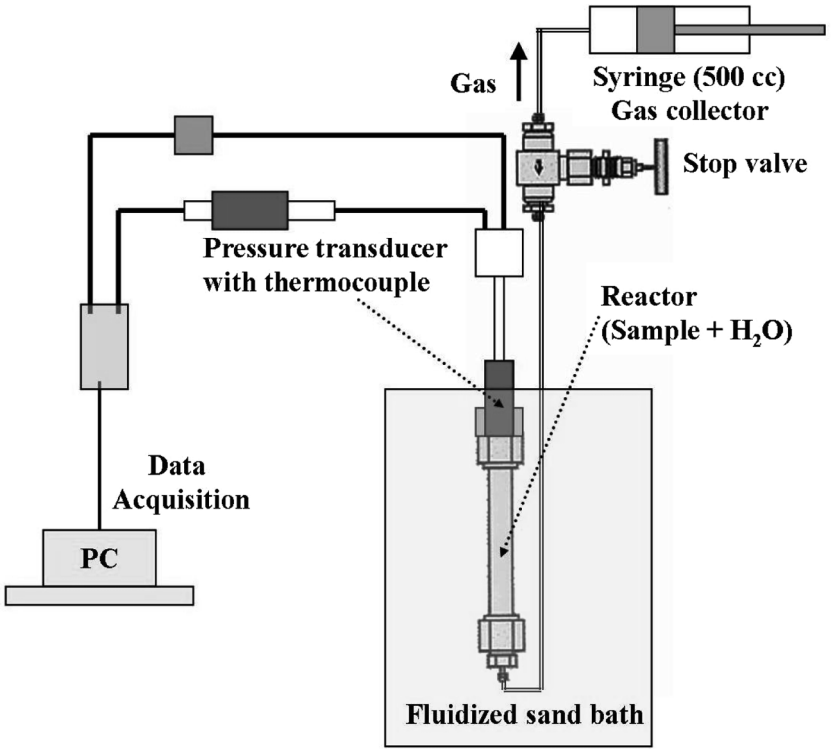

Fig. 2.7 A tubular batch reactor set-up in our lab

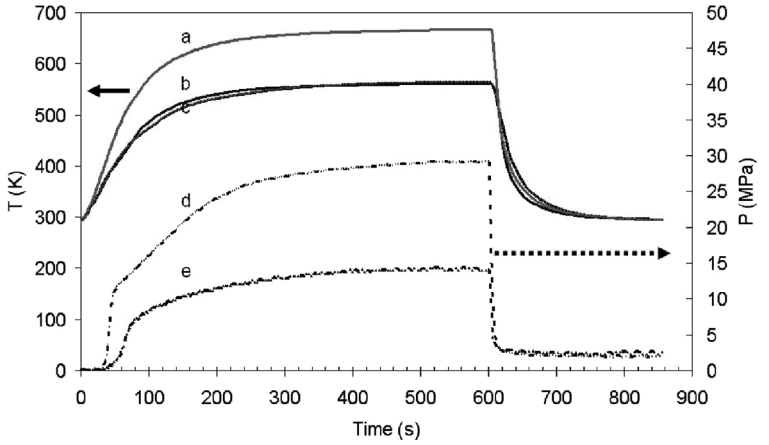

Fig. 2.8 Temperature and pressure profiles at different fluidized bed temperature (FBT) with or without H_2O_2 (49 wt%, 1 mL): **(a)** T at FBT = 673 K, **(b)** T at FBT = 573 K, **(c)** T at FBT = 573 K without H_2O_2, **(d)** P at FBT = 673 K, and **(e)** P at FBT = 573 K

Batch reactors are convenient for water-insoluble samples and long reaction time synthesis {e.g., several hours vs. 1 min in a flow reactor [24]} but not suitable for fast synthesis or some inorganic salt systems [25]. For example, the hydrolysis of acetate leads to the formation of acetic acid (boiling point of 391 K), which causes incontrollable increase of the pressure in the system. The temperature and concentration gradients as well as the slow rates for both heating and cooling lead to a non-uniform particle size distribution. But, the main advantages of batch reactors are (i) easy to design and operate; (ii) simple to increase reaction time for long time experiments {e.g., 25 h [26]}; and (iii) possible to control the oxidation states of the elements [25]. For example, copper hydroxy-carbonate decomposes into copper (II) oxide [25]:

$$(CuOH)_2CO_3 \rightarrow 2\ CuO\downarrow + CO_2 + H_2O \tag{2.8}$$

Oxalic acid under the same conditions decomposes with the formation of carbon monoxide:

$$H_2C_2O_4 \rightarrow CO + CO_2 + H_2O \tag{2.9}$$

The combination of these two reactions in SCW (658 K and 35 MPa) results in products of metallic copper (in the case of an excess of oxalic acid), a mixture of metallic copper and cuprous oxide (at salt/acid molar ratio = 1/2) and a mixture of copper (I) and copper (II) oxides (at salt/acid molar ratio = 3/1). The content of each phase is determined by the amount of oxalic acid added and, thus, can easily be controlled. Such a technique can be very efficient for preparation of catalysts and magnetic materials.

2.3 Flow Reactor

In contrast to batch systems, continuous flow reactors allow a better control of experimental conditions (e.g., temperature, pressure, time, concentration, pH and heating rate).

Figures 2.9 and 2.10 show a typical flow process and reactor used in Adschiri et al.'s work [16, 17] for hydrothermal crystallization of oxide nanoparticles. An aqueous metal salt solution [e.g., $Al(NO_3)_3$] is prepared and fed into the apparatus in one stream (Fig. 2.10: 4–6). In another stream, distilled water is pressurized and then heated to a temperature that is above the temperature desired (Fig. 2.10: 1–3, 6). The pressurized metal salt solution stream and the pure water stream are then combined in a mixing point (Fig. 2.10). This leads to rapid heating and subsequent reaction in the reactor (Fig. 2.10: 6). After the solution leaves the reactor, it is rapidly quenched by cold water and larger particles are removed by filters (Fig. 2.10: 6–11).

Pressure is controlled with a back-pressure regulator (Fig. 2.10: 10). The fine particles are collected in the effluent. Particles are separated and analyzed using the similar ways described in the above batch process. Conversion rate (%) is calculated

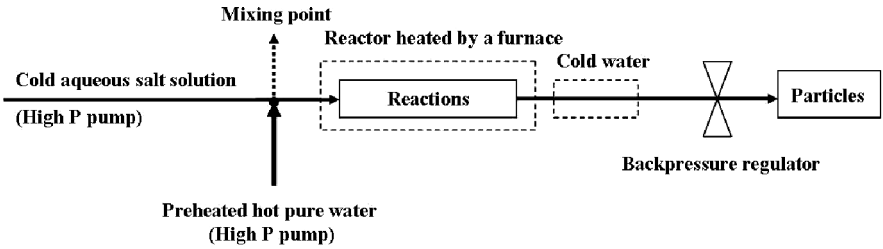

Fig. 2.9 A flow continuous process for rapid synthesis of fine particles in SCW

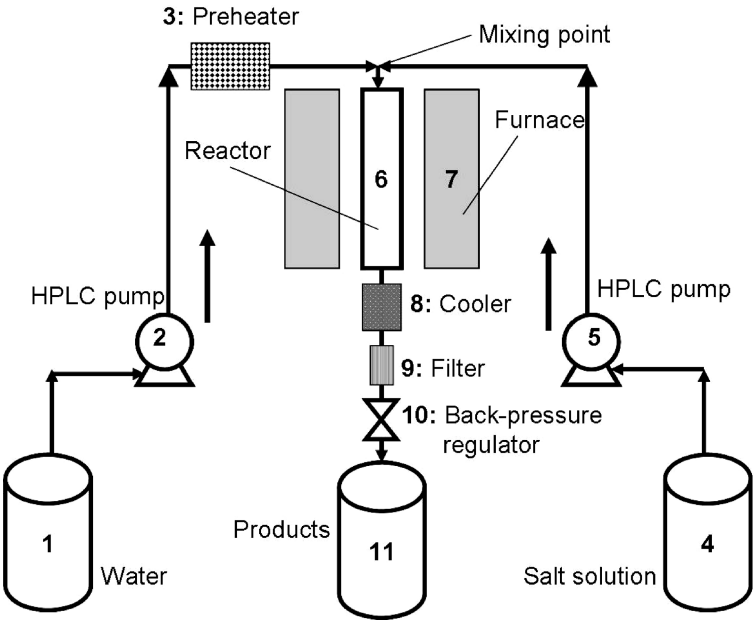

Fig. 2.10 A continuous flow reactor for rapid synthesis of fine particles in SCW

by dividing the difference between initial and final concentration of metal cation by its initial concentration. Productivity of the metal oxide particles is determined by the feed rate of the feed solution and conversion rate [21].

The reaction time (τ; min) is calculated by dividing the reactor volume (V; mL) by the flow rate at the reaction temperature (Q_r; mL/min):

$$\tau = V/Q_r \tag{2.10}$$

$$\tau = V(\rho_r/\rho_0)/Q_0 \tag{2.11}$$

Fig. 2.11 Image of the flow reactor built in our lab

where ρ_r represents the solution density at reaction temperature (kg/m^3), ρ_0 is the initial solution density (kg/m^3), and Q_0 is the initial flow rate (mL/min). Usually, τ is less than 2 min.

Figure 2.11 shows the image of a continuous flow reactor built in our lab with only one sample stream, without the preheated pure water stream (Fig. 2.10: 1–3).

2.4 Diamond Anvil Cell (DAC)

Another type of reactor, an optical micro-reactor (50 nL), Bassett-type diamond anvil cell (DAC; Figs. 2.12, 2.13, 2.14, 2.15, and 2.16) [27] that is widely used in hydrothermal systems for the study of minerals, polymers and biomass can be easily applied to the in-situ visual and micro-spectroscopic study of particle production by

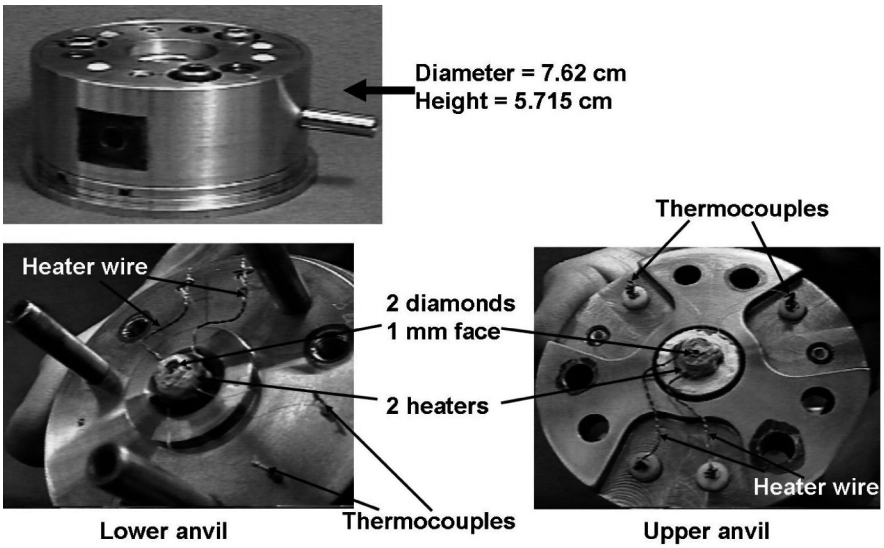

Fig. 2.12 Image of Bassett-type diamond anvil cell for the study of particle production in SCW

chemical synthesis and physical precipitation of solute from supercritical solution [27–30]. The DAC technique has the following merits: (i) clear visualization of the entire sample; (ii) access to spectroscopic techniques of FTIR/Raman/XRD to in-situ monitor reactions; (iii) high heating and cooling rates (± 20 K/s) due to small

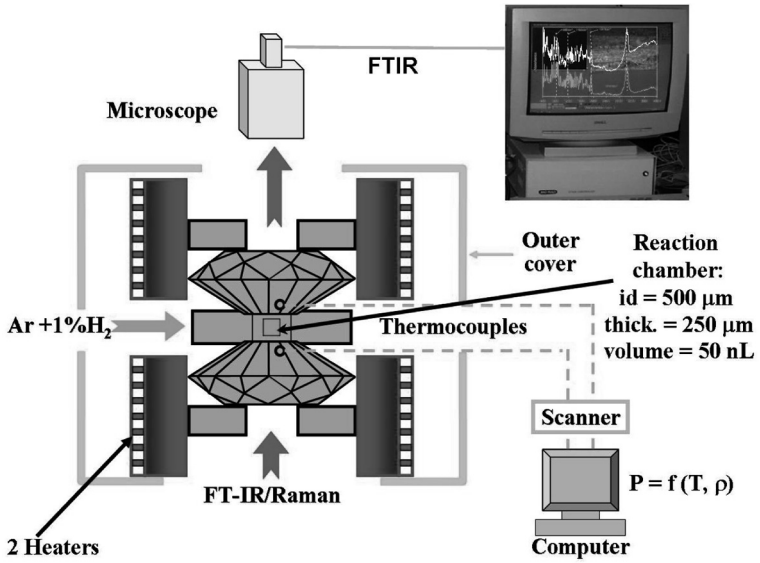

Fig. 2.13 Diamond anvil cell set-up system

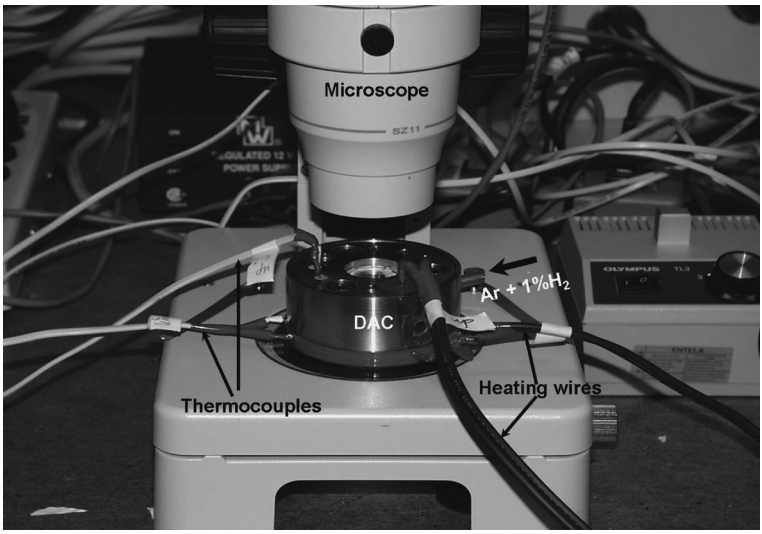

Fig. 2.14 Image of the DAC set-up ready for an experiment

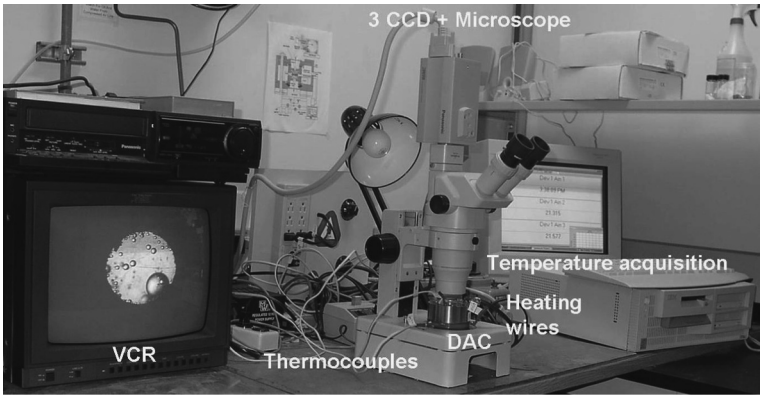

Fig. 2.15 Image of the DAC set-up system in experiment in our lab

volume; (iv) relatively inert materials in contact with the sample (diamonds, inconel gasket and ruby or ^{13}C diamond pressure sensor).

The DAC can be readily applied to hydrothermal systems at pressures up to 30 GPa and temperatures up to 1,473 K. Pressure is produced by two opposing diamond anvils inside the 50 nL chamber hole (internal diameter 508 μm, thickness 250 μm) made of inconel gasket (Fig. 2.13). Samples (solid) are loaded by placing solution (salt solutions, pure water, co-solvents) droplet into the gasket hole with a micro-syringe. The screw nuts of the DAC are tightened alternately in a 4-degree increment per turn, during which the samples are examined by an optical microscope (Olympus SZX16-3131) to check the loading. The samples and solution are heated

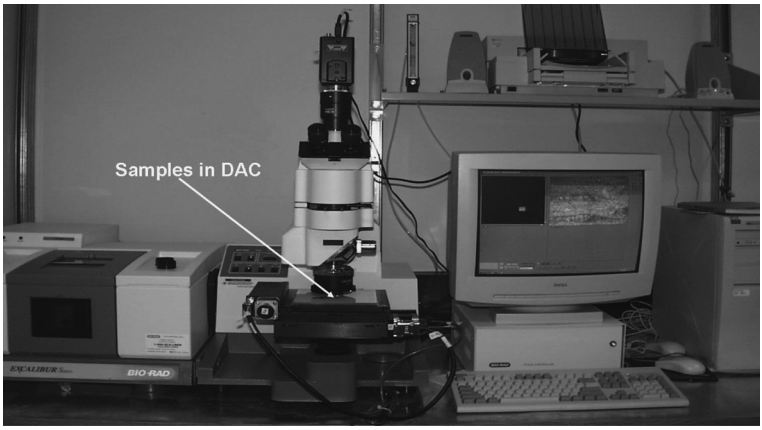

Fig. 2.16 FTIR micro-spectroscopy for analyzing samples from DAC

by two individual micro-heaters that transfer heat to the diamond anvils. Argon or nitrogen gas with 1% H_2 is introduced into the cell to protect the diamond anvils from oxidization and to increase the cooling rates at the end of the experiment.

Temperature is measured by two K-type thermocouples attached to each of the diamond anvils, and is recorded every 0.1 s by a data acquisition system (HP, Model 34970A). The thermocouples are calibrated by loading powder form samples contained in a gasket of reference metals tin ($T_m = 505.00$ K) and zinc ($T_m = 692.58$ K) and observing their melting points T_m with a slow heating rate (< 5 K/min).

The accuracy of the temperature measurement is estimated to be ± 0.5 K for temperatures up to 673 K, and ± 1.0 K for temperatures above 673 K. The temperature difference between the anvils is generally below 10 K (temperatures reported are the average of the both anvils) [31]. Pressure is determined from an EOSW [23] based on the negligible changes of chamber volume of the DAC, which was confirmed by Bassett [27] through the observation of the interference fringes between anvil faces radiated by a green light ($\lambda = 535$ nm). When the sample and water are loaded into the DAC chamber, Ar or N_2 gas bubbles will be introduced. Heating the chamber causes the liquid to expand and the gas bubbles to shrink until they disappear, at which point the chamber is filled with the expanded liquid at the homogenization temperature (T_h). The pressure at this point (P_h) is the vapor pressure along the liquid-vapor (L–V) curve of H_2O at T_h, and the bulk specific volume (υ_h) of the water is that of the liquid water along the L–V curve at T_h. If heated further, pressure will increase according to the P–T path of an isochore ($\upsilon = 1/\rho = \upsilon_h = \text{chamber} - \text{volume/water} - \text{mass};\ \text{m}^3/\text{kg}$). Thus, pressure can be calculated by knowing T at υ_h. The above calculation is assumed that only water contributes to the pressure. Figure 2.17 shows an example of temperature measured and pressure calculated in DAC.

At high water density (> 1,000 kg/m^3), pressure can be measured by ruby fluorescence R-lines of a ruby chip loading in the gasket hole [31, 32] with the equations

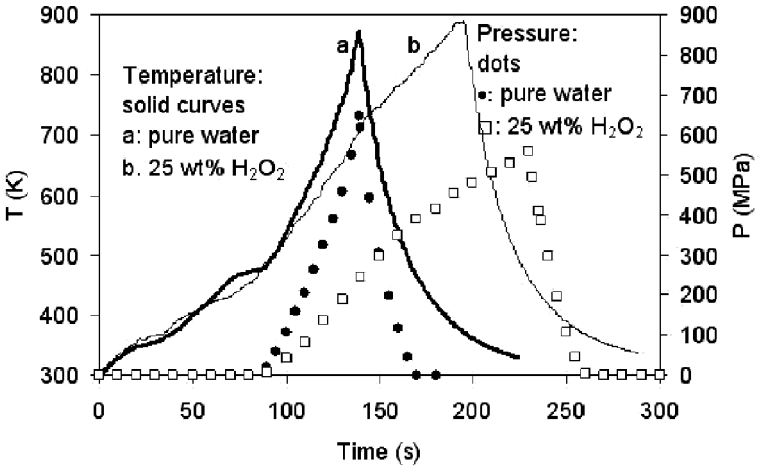

Fig. 2.17 Temperature (*solid curves*) measured and pressure (*dots*) calculated profiles vs. time in DAC with pure water (water density = 867 kg/m^3) and 25% H_2O_2 (water density = 917 kg/m^3)

of Forman et al. [33]:

$$P_1 = -(\varpi_1 - \varpi_{01})/0.77 \tag{2.12}$$

$$P_2 = -(\varpi_2 - \varpi_{02})/0.84 \tag{2.13}$$

where P and ϖ are the pressure and frequency of the ruby R_1 and R_2 lines having units of kbar and cm^{-1}, respectively. The $(\varpi_1 - \varpi_{01})$ and $(\varpi_2 - \varpi_{02})$ refer to the wave-number shift that occurs when the ruby is taken from room temperature and ambient pressure to the temperature and pressure of interest.

The ϖ is commonly determined by absolute methods, but relative values were used in our work [31, 32]. The fluorescence R-lines are conveniently measured with the Raman monochromator and the argon ion laser source. Pressure can be determined from either Eq. (2.12) or Eq. (2.13), but in our work, we used both R_1 and R_2 lines and determined pressure by averaging the values [31].

At higher temperatures, the formulas can be still used, provided the temperature dependent coefficient $\Delta\varpi/\Delta T$ is known. The coefficient has been shown to be independent pressure. In our experiments, we calibrated the coefficient over the range of 298∼696 K by measuring the shift change with temperature at atmospheric pressure, and the value used was [32]:

$$\Delta\varpi/\Delta T = 0.1363 \text{ cm}^{-1}/\text{K} \tag{2.14}$$

At temperatures higher than 818 K, the ruby R-lines disappear and ruby reacts slowly in SCW [34]. This reaction can be expected to increase at the higher temperatures. Therefore, pressure calibrated ^{13}C diamond can be used as the pressure sensor for these cases due to its inertness under high temperature conditions. The

equation used to determine the pressure is from Schiferl et al. [34]:

$$P = (\varpi - \varpi_0)/2.83 \text{ GPa} \quad (2.15)$$

where ϖ_0 is the Raman wavenumber (cm^{-1}) of ^{13}C diamond at ambient pressure and room temperature, and ϖ is the corresponding frequency at the given pressure.

The DAC screw nuts are adjusted prior to experiments to obtain the initial pressure desired. Samples (e.g., salt solution, biomass) are heated rapidly (e.g., 10 K/s) or slowly (e.g., 0.2 K/s) and observed at 110× magnification, and the images are recorded by a Panasonic 3CCD camera (AW-E350) in a computer or video cassette recorder (Figs. 2.14 and 2.15), and are analyzed with digital imaging to calculate the apparent concentration (area %) and phase transition and crystal growth rates. Reaction can be monitored by putting DAC in a microscope coupled with FT-IR (Fig. 2.16) or Raman spectroscopy (Varian 610-IR/Renishaw 3000 Raman microscope). After heating for a pre-determined time, the sample is rapidly cooled by cutting power to the heaters while maintaining Ar gas flow. The residues deposited on the diamond faces are analyzed by FT-IR/Raman microscopy and SEM. Details of experimental setup and procedures can be seen in our previous works summarized in the review paper [28] and book [29].

References

1. T. Masui, Y. Peng, K. Machida, G. Adachi, Reduction behavior of CeO_2–ZrO_2 solid solution prepared from cerium zirconyl oxalate. Chem. Mater. **10**, 4005–4009 (1998)
2. M. Yashima, K. Morimoto, N. Ishizawa, M. Yoshimura, Zirconia-ceria solid solution synthesis and the temperature-time-transformation diagram for the 1:1 composition. J. Am. Ceram. Soc. **76**, 1745–1750 (1993)
3. C. de Leitenburg, A. Trovarelli, F. Zamar, S. Maschio, G. Dolcetti, J. Llorca, A novel and simple route to catalysts with a high oxygen storage capacity: The direct room-temperature synthesis of CeO_2–ZrO_2 solid solutions. J. Chem. Soc. Chem. Commun. **21**, 2181–2182 (1995)
4. A. Deptula, M. Carewska, T. Olczak, W. Lada, F. Croce, Sintering of zirconia-ceria spherical powders prepared by a water extraction variant of the sol-gel process. J. Electrochem. Soc. **140**, 2294–2297 (1993)
5. S. Hirano, T. Yogo, K. Kikuta, E. Asai, K. Sugiyama, H.Yamamoto, Preparation and phase separation behavior of cobalt iron oxide ($(Co,Fe)_3O_4$) films. J. Am. Ceram. Soc. **76**, 1788–1792 (1993)
6. J.F. Hochepied, P. Bonville, M.P. Pileni, Nonstoichiometric zinc ferrite nanocrystals: syntheses and unusual magnetic properties. J. Phys. Chem. B **104**, 905–912 (2000)
7. T. Masui, K. Fujiwara, Y. Peng, T. Sakata, K. Machida, H. Mori, G. Adachi, Characterization and catalytic properties of CeO_2–ZrO_2 ultrafine particles prepared by the microemulsion method. J. Alloys Compd. **269**, 116–122 (1998)
8. M. Kiyama, The formation of manganese and cobalt ferrites by the air oxidation of aqueous suspensions and their properties. Bull. Chem. Soc. Jpn. **51**, 134–138 (1978)
9. T. Kodama, Y. Wada, T. Yamamoto, M. Tsuji, Y. Tamaura, Synthesis and characterization of ultrafine nickel(II)-bearing ferrites ($Ni_xFe_{3-x}O_4$, x = 0.14–1.0). J. Mater. Chem. **5**, 1413–1418 (1995)
10. B. Djuricic, D. McGarry, S. Pickering, The preparation of ultrafine ceria-stabilized zirconia particles coated with yttria. J. Mater. Sci. Lett. **12**(16), 1320–1323 (1993)

11. A. Cabanas, M. Poliakoff, The continuous hydrothermal synthesis of nano-particulate ferrites in near critical and supercritical water. J. Mater. Chem. **11**, 1408–1416 (2001)
12. G.W. Morey, P. Niggli, Hydrothermal formation of silicates, a review. J. Am. Chem. Soc. **35**, 1086–1130 (1913)
13. A. Rabenau, The role of hydrothermal synthesis in preparative chemistry. Angew. Chem. **97**, 1017–1032 (1985)
14. R. Gainsford, M.J. Sisley, T.W. Swaddle, P. Bayliss, Hydrothermal formation of ferrite spinels. Can. J. Chem. **53**, 12–19 (1975)
15. H. Kumazawa, K. Oki, H.M. Cho, E. Sada, Hydrothermal synthesis of ultrafine ferrite particles. Chem. Eng. Commun. **115**, 25–33 (1992)
16. T. Adschiri, K. Kanazawa, K. Arai, Rapid and continuous hydrothermal synthesis of boehmite particles in subcritical and supercritical water. J. Am. Ceram. Soc. **75**, 2615–2618 (1992)
17. T. Adschiri, K. Kanazawa, K. Arai, Rapid and continuous hydrothermal crystllization of metal oxides particles in supercritical water. J. Am. Ceram. Soc. **75**, 1019–1022 (1992)
18. K. Sue, N. Kakinuma, T. Adschiri, K. Arai, Continuous production of nickel fine particles by hydrogen reduction in near-critical water. Ind. Eng. Chem. Res. **43**(9), 2073–2078 (2004)
19. R.L. Smith Jr., P. Atmaji, Y. Hakuda, Y. Kawaguchi, T. Adschiri, K. Arai, Recovery of metals from simulated high-level liquid waste with hydrothermal crystallization. J. Supercrit. Fluids **11**(1,2), 103–114 (1997)
20. Z. Fang, S.K. Xu, J.A. Kozinski, Behavior of metals during combustion of industrial organic wastes in supercritical water. Ind. Eng. Chem. Res. **39**(12), 4536–4542 (2000)
21. T. Adschiri, Y. Hakuta, K. Arai, Hydrothermal synthesis of metal oxide fine particles at supercritical conditions. Ind. Eng. Chem. Res. **39**, 4901–4907 (2000)
22. Inorganic Chem. group, Dalian S&T university, *Inorganic Chemistry* (in Chinese) (Higher education press, Beijing, China, 1990), p. 645
23. W. Wagner, A. Pruss, The IAPWS formulation 1995 for the thermodynamic properties of ordinary water substance for general and scientific use. J. Phys. Chem. Ref. Data **31**(2), 387–535 (2002)
24. Y. Hakuta, T. Adschiri, T. Suzuki, T. Chida, K. Seino, K. Arai, Flow method for rapidly producing barium hexa-ferrite particles in supercritical water. J. Am. Ceram. Soc. **81**, 2461–2464 (1998)
25. A.A. Galkin, B.G. Kostyuk, N.N. Kuznetsova, A.O. Turakulova, V.V. Lunin, M. Polyakov, Unusual approaches to the preparation of heterogeneous catalysts and supports using water in subcritical and supercritical states. Kinetika i kataliz **42**, 172–181 (2001)
26. R.B. Yahya, H. Hayashi, T. Nagase, T. Ebina, Y. Onodera, N. Saitoh, Hydrothermal synthesis of potassium hexatitanates under subcritical and supercritical water conditions and its application in photocatalysis. Chem. Mater. **13**, 842–847 (2001)
27. W.A. Bassett, A.H. Shen, M. Bucknum, I.M. Chou, A new diamond-anvil cell for hydrothermal studies to 2.5 GPa and from –190 °C to 1200 °C. Rev. Sci. Instrum. **64**, 2340–2345 (1993)
28. R.L. Smith Jr., Z. Fang, Techniques, applications and future prospects of diamond anvil cells for studying supercritical water systems. J. Supercrit. Fluids **47**, 431–446 (2009)
29. Z. Fang, *Complete Dissolution and Oxidation of Organic Wastes in Water*, VDM Verlag Dr. Müller Aktiengesellschaft & Co. KG, Saarbrücken, Germany, ISBN 9783639144246, 192 pages, Apr. 2009.
30. H. Assaaoudi, Z. Fang, I.S. Butler, J.A. Kozinski, Synthesis of erbium hydroxide microflowers and nanostructures in subcritical water. Nanotechnolgy **19**, 185606 (8 pp) (2008)
31. Z. Fang, R.L. Smith Jr., H. Inomata, K. Arai, Phase behavior and reaction of polyethylene terephthalate-water systems at pressures up to 173 MPa and temperatures up to 490 °C. J. Supercrit. Fluids **15**, 229–243 (1999)
32. Z. Fang, R.L. Smith Jr., H. Inomata, K. Arai, Phase behavior and reaction of polyethylene in supercritical water at pressure up to 2.6 GPa and temperature up to 670°C. J. Supercrit. Fluids **16**, 207–216 (2000)

33. R.A. Forman, G.J. Piermarini, J.D. Barnett, S. Block, Pressure measurement made by the utilization of ruby sharp-line luminescence. Science **176**, 284–285 (1972)
34. D. Schiferl, M. Nicol, J.M. Zaug, S.K. Sharma, T.F. Cooney, S.-Y. Wang, T.R. Anthony, J.F. Fleischer, The diamond $^{13}C/^{12}C$ isotope Raman pressure sensor system for high-temperature/pressure diamond-anvil cells with reactive samples. J. Appl. Phys. **82** 3256–3265 (1997)

http://www.springer.com/978-3-642-12986-5

Rapid Production of Micro- and Nano-particles Using Supercritical Water

Fang, Z.

2010, XXVIII, 92 p. 84 illus., 14 illus. in color., Hardcover
ISBN: 978-3-642-12986-5